UNIVERSITY OF CALIFORNIA
RIVERSIDE

Skyrmion Dynamics for Spintronic Devices

A Thesis submitted in partial satisfaction
of the requirements for the degree of

Master of Science

in

Electrical Engineering

by

Yizhou Liu

December 2013

Thesis Committee:

Professor Roger Lake, Chairperson
Professor Alexander Khitun
Professor Ming Liu

The Thesis of Yizhou Liu is approved:

Committee Chairperson

University of California, Riverside

Acknowledgments

I would like to first thank my graduate advisor Prof. Roger Lake, Department of Electrical Engineering UC Riverside for his guidance and useful suggestions. It's also my honor to working with all members from LATTE at UC Riverside. I also want to acknowledge Dr. Jiadong Zang for his explanation in some physical concepts. Thanks for my parents and Yijing Bian for encouraging and supporting me to continue my graduate education.

ABSTRACT OF THE THESIS

Skyrmion Dynamics for Spintronic Devices

by

Yizhou Liu

Master of Science, Graduate Program in Electrical Engineering
University of California, Riverside, December 2013
Professor Roger Lake, Chairperson

Magnetic Skyrmion is a topological stable, particle-like spin texture. Its unique properties such as curren-driven motion and topological protected make it to be a candidate for future spintronic devices. However, Skyrmion dynamics are still not that clear to build real devices. To investigate those Skyrmion dynamics, a code was developed to solving the Landau-Lifshitz-Gilbert Equation. Skyrmion dynamics with spin waves is investigated by micromagnetic simulations, we find that the scattering angle of the spin wave is related to the size of Skyrmion. We also show the simulation of the topological hall effect that maybe used to read a Skyrmion. Based on the current dynamic properties of Skyrmion, we proposed a Skyrmion-based architecture.

Contents

List of Figures

Chapter 1

Motivation

In recent years, electronic devices such as CPU and memory get faster and smaller. However, the speed improvement seems not that obviously compare to 10 years before. The silicon-based electronic devices are almost reach their physical limit. The scale of these devices is a problem when the size is down to sub-10nm, there will be quantum effect that is hard to control. So more and more researchers are now focusing on finding new pathway to build next generation devices. There are some candidates for next generation devices such as the magnetic-tunneling junction[6], domain wall race-track memory[5], carbon nanotube(CNT) based computing unit[7] and also the quantum computing[8]. So it's really necessary to find a new candidate technology to get over the current bottleneck in electronic devices.

Magnetic Skyrmion, which is a topological protected spin texture, gains a lot of interest in recent years. It has some unique properties such as the particle like behavior, current-driven motion[9]. And since it's topological protected, a defect cannot stop the motion of Skyrmion[10]. It's also known that we can control the Skyrmion motion by a electric field in a insulator, which maybe a solution for making devices

without joule heat[1]. But there are still some open questions of its properties need to be solved, especially the dynamics behavior, before we build real Skyrmion-based devices. So inspired by these open questions, we investigate some Skyrmion dynamics by micromagnetic simulations and propose some possible architectures for Skyrmion-based spintronic devices.

Chapter 2

Magnetism

Since magnetic Skyrmion is a topological protected spin texture, the origin of Skyrmion should be the magnetism. Magnetism has been known for such a long time by human beings. However, after entering the 20th century, there is more researches on the micromagnetism and the quantum theory of magnetism. So to understand the physics of magnetic Skyrmion I want to introduce some concepts of magnetism first in this chapter.

2.1 Bohr Magneton and Magnetic Moment

Bohr model in atomic physics was introduced by Niels Bohr in 1913. The emergence of Bohr model gives physicist a rational picture of the atom structure. In this picture, the electron in a hydrogen atom with mass m and charge -e(which e is the proton charge). The electrostatic force on the electron should equal to the centripetal force to hold the electron in its circular orbit with a radius r, as shown in Eq. (2.1):

$$\frac{e^2}{4\pi\varepsilon_0 r} = \frac{mv^2}{r} \tag{2.1}$$

Bohr model proposed that the electron can only stay in one of a number of discrete orbits to keep orbit stably without radiating. Then we will have the assumption in Eq. (2.2)

$$mvr = n\hbar \tag{2.2}$$

with $n = 1, 2, 3, ...$, where $\hbar$ is the reduced Planck's constant. By Eq. (2.1) and Eq. (2.2), we can eliminate v to obtain r and then find the total energy:

$$r = n^2 \frac{4\pi\varepsilon_0\hbar^2}{me^2} = n^2 a_0, \qquad E_n = -\frac{1}{n^2}\frac{e^4 m}{2(4\pi\varepsilon_0)^2\hbar^2} \tag{2.3}$$

$a_0 (= 0.5292 \times 10^{-10}$ m) is the well known Bohr radius. The energy gap between two neighbor orbits is $hf = E_1 - E_2$, which f is the frequency and E_1, E_2 are two energy states associate with these two orbits.

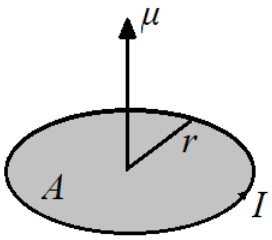

Figure 2.1: Illustration of a magnetic moment and its current loop.

The classical expression of a magnetic moment for an electron is $\mu = IA$. The effective current induced by this electron can be written as $I = -\frac{e}{T}$, where $T (= \frac{2\pi r}{v})$ is the period of orbit. Using the equations above we obtain

$$\mu_B = \frac{|e|\hbar}{2m} \tag{2.4}$$

$\mu_B = 9.2740 \times 10^{-24}$ J/T is a unit of magnetic moment so called the Bohr magneton.

Furthermore we can show that the ratio

$$\frac{\mu}{L} = \gamma = -\frac{e}{2m} \tag{2.5}$$

between magnetic moment μ and angular momentum L depends only on basic constants. This ratio, γ, is called the gyromagnetic ratio, and will be used in the later chapters.

2.2 Magnetic Interaction

Magnetic structures such as domain wall, magnetic vortex could be found in magnets and used for applications. To study these magnetic structures we need to understand the origin of a magnetic structure or a magnetic phenomena. The theory of micromagnetism is still unknown until the early 20th century. After the discovery of electrons and the foundation of quantum theory, it became possible to describe these magnetic structures clearly by magnetic interaction and gave us a vision into the origin of micromagnetism.

2.2.1 Heisenberg Exchange Interaction

The Heisenberg exchange is rising from the interaction between two electrons. Consider a simple case that two electrons with different spatial coordinates r1 and r2. The coupling of the two electrons will give a rise to the Hamiltonian that can be written as:

$$H = J \cdot \mathbf{S}_i \cdot \mathbf{S}_j \tag{2.6}$$

where $\mathbf{S}_i$ and $\mathbf{S}_j$ are the spin operators of these two electrons. Since electron has a spin $\frac{1}{2}$, the total spin of this system $\mathbf{S}_{tot} = \mathbf{S}_i + \mathbf{S}_j$ has an eigenvalue of either 0 or 1. Then we can have

$$(\mathbf{S}_{tot})^2 = (\mathbf{S}_i)^2 + (\mathbf{S}_j)^2 + 2 \cdot \mathbf{S}_i \cdot \mathbf{S}_j \tag{2.7}$$

the eigenvalue of $(\mathbf{S}_{tot})^2$ could be either 0 or 2 for spin 0 or 1 respectively. Because we know the eigenvalue of $(\mathbf{S}_i)^2$ and $(\mathbf{S}_j)^2$ are both $\frac{3}{4}$, we can easily obtain $\mathbf{S}_i \cdot \mathbf{S}_j$ by Eq. (2.7)

$$\mathbf{S}_i \cdot \mathbf{S}_j = \begin{cases} \frac{1}{4} & for s = 1 \\ -\frac{3}{4} & for s = 0 \end{cases} \tag{2.8}$$

take those values back to Eq. 2.6, the eigenvalues of the Hamiltonian are

$$E = \begin{cases} \frac{J}{4} & for s = 1 \\ -\frac{3J}{4} & for s = 0 \end{cases} \tag{2.9}$$

The degeneracy of each state can be given by $2s + 1$, so the $s = 0$ state is the singlet state and the $s = 1$ state is the triplet state. Hence we can write the wavefunction of these two states as

$$\begin{aligned} \Psi_S &= \tfrac{1}{\sqrt{2}} \left[\phi_i(\mathbf{r}_1)\phi_j(\mathbf{r}_2) + \phi_i(\mathbf{r}_2)\phi_j(\mathbf{r}_1)\right] \chi_S \\ \Psi_T &= \tfrac{1}{\sqrt{2}} \left[\phi_i(\mathbf{r}_1)\phi_j(\mathbf{r}_2) - \phi_i(\mathbf{r}_2)\phi_j(\mathbf{r}_1)\right] \chi_T \end{aligned} \tag{2.10}$$

and the energy difference between these two states is

$$E_S - E_T = 2 \int \phi_i^*(\mathbf{r}_1)\phi_j^*(\mathbf{r}_2) H \phi_i(\mathbf{r}_2)\phi_j(\mathbf{r}_1) \mathbf{dr_1 dr_2} \tag{2.11}$$

We define the exchange constant J as

$$J = \frac{E_S - E_T}{2} = \int \phi_i^*(\mathbf{r}_1)\phi_j^*(\mathbf{r}_2) H \phi_i(\mathbf{r}_2)\phi_j(\mathbf{r}_1) \mathbf{dr_1 dr_2} \tag{2.12}$$

Hence the Hamiltonian can be finally written as

$$H = -2J \cdot \mathbf{S}_i \cdot \mathbf{S}_j \tag{2.13}$$

If $J > 0$, $E_S > E_T$ means the triplet state($\mathbf{S} = 0$) is in lower energy and the neighbour spins intend to be parallelized each other to form the ferromagnetic(FM). If $J < 0$, $E_S < E_T$ means the singlet state($\mathbf{S} = 1$) is in lower energy and the neighbour spins intend to

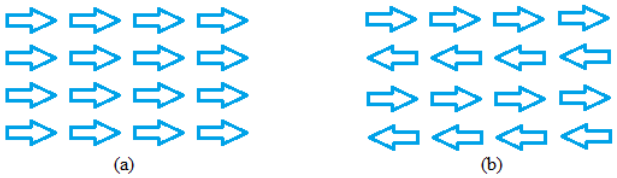

Figure 2.2: (a) Ferromagnetic State(FM). (b) Antiferromagnetic State(AFM)

be antiparallelized each other to form the antiferromagnetic(AFM). Furthermore, Eq. (2.13) can be written in a more general way

$$H = -\sum_{i,j} J_{ij}\mathbf{S}_i \cdot \mathbf{S}_j \tag{2.14}$$

where J_ij is the exchange constant between two sites i and j. This form is usually used in solid state physics and so called the classical Heisenberg model.

2.2.2 Dzyaloshinskii-Moriya Interaction

The interaction due the broken of symmetry is called the Dzyaloshinskii-Moriya interaction[11, 12]. Due to the observation of some complex, non-linear spin textures, the DM interaction becomes more and more important in the comparison of material properties. The DM interaction was first proposed by I. Dzyaloshinskii in 1958 and T. Moriya generalized this theory two years later. By Moriya's theory we could determine the direction of the DM interaction. A normal expression of a DM interaction is $H = \mathbf{D}_{12} \cdot (\mathbf{S}_1 \times \mathbf{S}_2)$, where D is the DM constant. Under the inversion operation, two spins $\mathbf{S}_1$ and $\mathbf{S}_2$ are exchanged. The cross product reverses the sign of the Hamiltonian. The DM interaction is the key factor to generate a Skyrmion and we will discuss it in details in the following chapters.

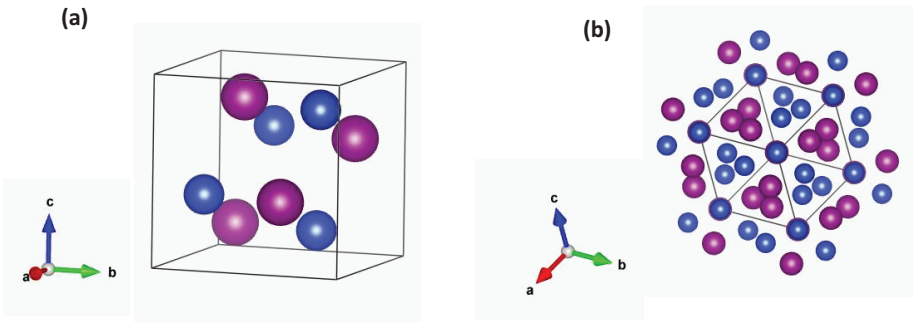

Figure 2.3: (a) The unit cell of MnSi. (b) The (111) face of MnSi lattice. Pink balls stand for Mn atoms, and the blue balls stand for the Si atoms.

2.3 Zeenman Energy

Magnetic structure is not only the result of magnetic interactions, but also the result of external applied field. The interaction of an atom with a magnetic field is called the Zeeman energy. It's caused by the spin of the electrons in an atom. The Zeeman energy is given by:

$$H = -h_0 \cdot m \tag{2.15}$$

where h_0 is the external field and m is the magnetic moment.

Chapter 3

Magentic Skyrmion

In 1962, Tony Skyrme proposed that protons and neutrons exist as topological solitons[13]. These solitons are particle-like field configurations. And since they are topological protected, their structures are stable and cannot deformed continuously. This concept is applied in many fields such as particle physics and condensed-matter physics, and this kind of solitons is called Skyrmion.

3.1 Magnetic Skyrmion

Magnetic skyrmions are topologically protected, particle-like spin textures. They range in sizes from 10 nm to approximately 100 nm depending on material parameters. They can be created and annihilated by spin currents and magnetic fields, and they can be easily moved by an electrical current [14, 10]. In many materials, skyrmions are the middle phase of a progression of three phases with increasing magnetic field: helical, skyrmion, and ferromagnetic [15]. Because of the their small size, their stability, the demonstration of their individual creation and annihilation, and their facile movement with low current, they are being investigated for information storage (memory)

applications [10].

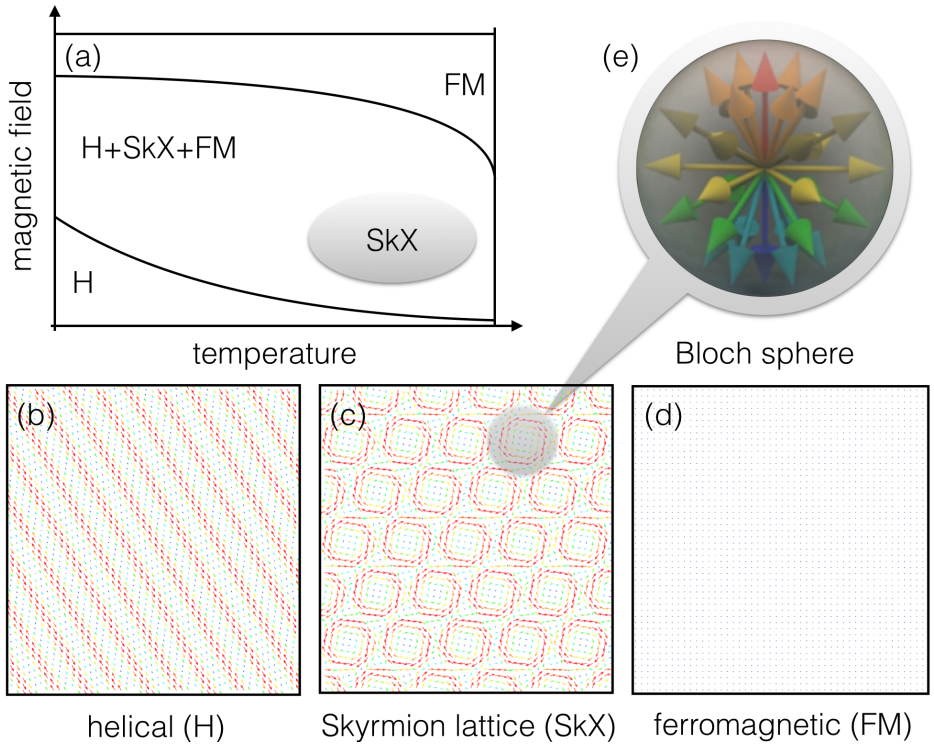

Figure 3.1: (a) Phase diagram of a helimagnet. The Skyrmion crystal occurs at finite temperature and moderate magnetic fields. (b) Helical phase. (c) Skyrmion lattice. (d) Ferromagnetic phase. (e) Bloch sphere showing the spins of a Skyrmion.

The origin of a magnetic Skyrmion is the Dzyaloshinskii-Moriya interaction and its competition with other magnetic interactions such as the exchange interaction. The Dzyaloshinskii-Moriya interaction $H = \mathbf{D}_{12} \cdot (\mathbf{S}_1 \times \mathbf{S}_2)$ comes from inversion symmetry breaking and spin-orbit interaction. Under the inversion operation, two spins $\mathbf{S}_1$ and $\mathbf{S}_2$ are exchanged. The cross product reverses the sign of the Hamiltonian. Up to now, most bulk materials for Skyrmion crystal belong to the category of B20 compounds, whose space group is $P2_13$. Although they are cubic lattices, the symmetry is very low due to the complicated structures inside each unit cell. The inversion symmetry is missing consequently. Another route to the Dzyaloshinskii-Moriya interaction is to grow magnetic thin films on certain substrates. The inversion symmetry is apparently

broken due to different chemical environments above and below that thin film. On the

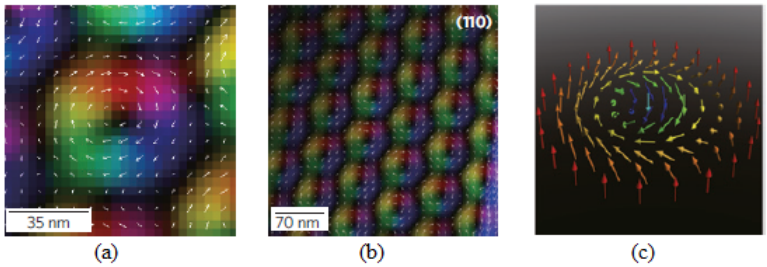

Figure 3.2: (a)A single Skyrmion observed by Lorentz microscopy (b) Skyrmion lattic (c)Spin plot of a Skyrmion.[1]

other hand, the amplitude of the Dzyaloshinskii-Moriya interaction is proportional to the strength of spin-orbit interaction. Therefore it is better to use materials with large spin-orbit interaction as the substrate.

3.2 Skyrmion Lattice

The first magnetic Skyrmion was observed in MnSi which is a phase between the helical state and ferromagnetic state. By the presence of a finite external field, a Skyrmion phase will be generated. The Skyrmions were arranged as a hexagonal like lattice on the plane perpendicular to the external field.

The phase diagram of MnSi bulk sample is shown in Fig. 3.3. At low temperature, when the magnetic field is high enough, local spins are fully polarized so that ferromagnetic order is respected. When the magnetic field is reduce, the conical phase is energetically favored. In this phase, the spins are propagating in the $\hat{z}$ direction and rotating about the z axis like an umbrella. The net magnetization is nonzero so that energy can still be saved from the Zeeman coupling. This phase is the result of compro-

mise between Zeeman interaction and Dzayloshinskii-Moriya interaction. Furthermore, once the magnetic field is sufficiently small, Zeeman coupling is no longer relavent, and the competition between ferromagnetic exchange and Dzyaloshinskii-Moriya interaction is important. As a result, the helical phase has the lowest energy. In this phase, the spins are coplanar and can propagate in any direction.

The Skyrmion crystal phase (SkX), the so-called A phase in previous literatures, is present at finite temperature. Compared to the conical phase, the free energy of the Skyrmion crystal phase can be reduced due to thermal fluctuations. Mühlbauer et al. performed a neutron scattering analysis of this phase[15]. They found six bright spots forming a hexagon in the momentum space. More importantly, the separation between the bright spots and the Γ point is much smaller than the Brillions zone boundary of the original lattice. All these signals indicate that the Skyrmions form a triangle lattice in this phase.

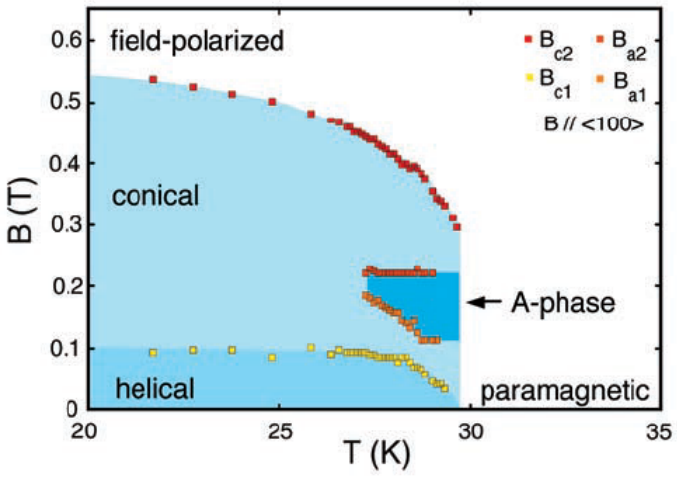

Figure 3.3: A Phase diagram of MnSi.[2]

In order to further confirm the Skyrmion phase by real space imaging, $Fe_{0.5}Co_{0.5}Si$ thin film is studied by means of Lorentz Transmission Electron Microscopy[16]. In contrast to the bulk sample, the conical phase is no longer present due to the geometric confinement in the directioin perpendicular to the thin film. In this case, Skyrmions can survive down to zero temperature. The Skyrmion crystal phase is really the groundstate of the spin system as long as the magnetic field is properly chosen.

Around the boundary between ferromagnetic phase and the Skyrmion phase, Yu et al. observed the coexistence of both phases[16]. The Skyrmion crystal is melted and single Skyrmion can be observed. This phenomenon shows similarity to the solid-liquid phase transition and indicates the transition from ferromagnetic phase to the Skyrmion crystal phase is first order. The same behavior appears at the transition between the helical phase and the Skyrmion crystals phase. Therefore this phase is first order as well.

All these properties of helimagnet thin film can be captured by the following simple Hamiltonian on two dimensional square lattice[17, 16]. The magnetic orders of this Hamiltonian are simply stacked along the direction perpendicular to the film.

$$H = \sum_{\langle ij \rangle} [-J\mathbf{S}_i \cdot \mathbf{S}_j + \mathbf{D}_{ij} \cdot (\mathbf{S}_i \times \mathbf{S}_j)] - \sum_i \mathbf{H} \cdot \mathbf{S}_i \tag{3.1}$$

where the first term is the Heisenberg ferromagnetic exchange, the second term is the Dzyaloshinskii-Moriya interaction, and the last term is the Zeeman coupling between magnetic moments $\mathbf{S}_i$ and the external magnetic field $\mathbf{H}$. Here the Dzyaloshinskii-Moriya vector $\mathbf{D}_{ij}$ is chosen, due to the lattice symmetry, to be $D\hat{\mathbf{r}}_{ij}$, where the scalar D describes the interaction strength, and $\hat{\mathbf{r}}_{ij}$ is the unit vector pointing from site i to site j. All other anisotropy terms and dipolar-dipolar interaction are negligible in the usual cases with small D, the Skyrmion radius or helical period is proportional to $(J/D)a$,

where a is the lattice constant, and the critical field separating the ferromagnetic phase and Skyrmion phase is about $D^2/J\mu_B$[17]. Usually, the Skyrmion radius ranges from 10 to 100nm, and the critical field ranges from 100 to 1000G. It provides the possibility of realizing ultradense and low-disspative memory devices.

Recently, the magnetic Skyrmion also has been observed in a multiferroic material Cu_2OSeO_3, which is also a insulator[1]. Cu_2OSeO_3 is also a B20 material that lack the center symmetric of inversion. The crystal structure of a Cu_2OSeO_3 is shown in Fig. 3.4 Since this material is an insulator, we can use electric field instead of a electric

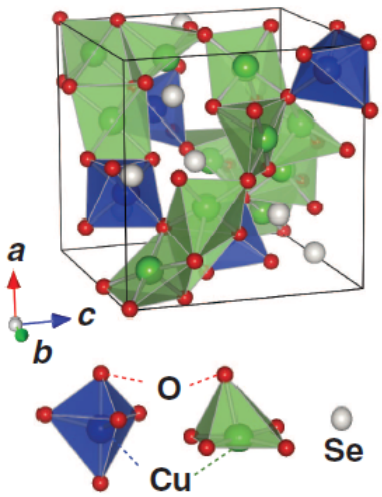

Figure 3.4: Crystal structure of Cu_2OSeO_3.[1]

current to manipulate the Skyrmion and without losses due to the joule heating.

3.3 Skyrmion Dynamics

Skyrmion can be driven by a current or a electrical field in a insulator. Another interesting dynamics property is that a defect cannot stop the motion of a Skyrmion[10]. This property maybe useful when modify Skyrmion in a real devices. The current density need to move a Skyrmion is just about 10^6 A/m which is 5 orders small than moving a domain wall. That's one reason why people are really interested in Skyrmion. As shown in Fig. 3.5 When a conduction electron passes through a Skyrmion, its spin

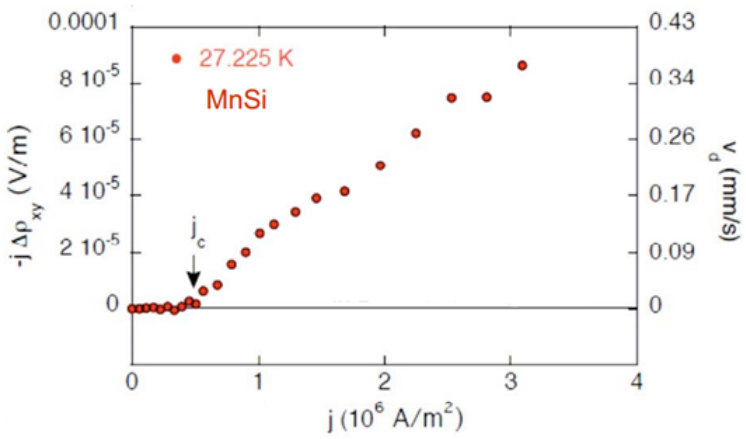

Figure 3.5: Plot of Skyrmion velocity vs current density.[3]

is fully polarized by the spin texture which generates a Berry phase that effectively corresponds to a flux quanta, $\phi = h/e$.[18, 16, 19, 3, 20]. This so-called "emergent guage field" produces a Magnus force perpendicular to the skyrmion velocity as shown in Fig. 3.6, which eventually generates a topological Hall effect. For FeGe, the Skyrmion radius R is about 20nm[21, 22]. The corresponding average emergent magnetic field $b \sim h/e\pi R^2 \approx 3.5$T. For the atomic scale Skyrmion Fe/Ir(111)[23], the average field can

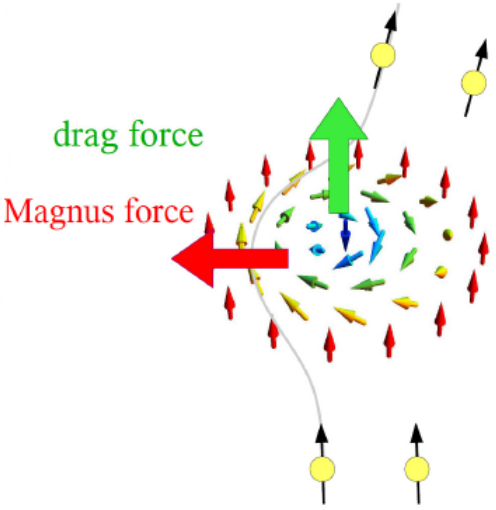

Figure 3.6: Magnus Force.[4]

be as large as several hundred Tesla. Skyrmion crystal automatically provides a high magnetic field laboratory.

Such a high, effective magnetic field naturally results in a Hall effect of the itinerant electrons. However, this topological Hall effect depends on the validity of the adiabatic approximation. When the conduction electron's kinetic energy is comparable to its exchange coupling to the magnetic moments, perfect alignment between the electron spin and the magnetic moment is no longer the case. Furthermore, a hopping electron provides spin transfer torque, to the magnetic moment.

Chapter 4

Skyrmion dynamic simulation

Since Skyrmion is a topological protected spin texture, its dynamic properties are worth to investigate. Also if we want to make Skyrmion-based devices, it's necessary to know these kind of properties such as the formation process of a single Skyrmion, current-driven motion, etc. In this chapter, we will discuss the Skyrmion dynamics by micromagnetic simulations.

4.1 Theoretical Background

To investigate the dynamics of Skyrmion, we need to employ the Landau-Lifshitz-Gilbert Equation in our code. The standard expression of a Landau-Lifshitz-Gilbert Equation can be written as:

$$\dot{\mathbf{S}} = -\gamma \mathbf{S} \times \mathbf{H}_{eff} + \alpha \mathbf{S} \times \dot{\mathbf{S}} \tag{4.1}$$

where S is the magnetization, also known as magnetic moment per unit volume, The magnitude of the spin $\mathbf{S}$ is normalized to unity. α is the Gilbert damping constant, γ is the gyromagnetic ratio and $\mathbf{H}_{eff}(= -\partial H/\partial \mathbf{S})$ is the effective field acting on the local magnetic moment $\mathbf{S}$. The in-plane magnetic field is included in this effective field.

Starting from a ferromagnetic initial state, we will apply the fourth order Runge-Kutta method to numerically integrate this first differential equation.

Furthermore, if we want to simulating the creation of a single Skyrmion, it is also important to discuss the effect of finite temperatures. Because to create a single Skyrmion, a typical method is applied a current which will generally heat the whole system. To this end, a stochastic Landau-Lifshitz-Gilbert approach will be employed. The equation of motion is given by

$$\dot{\mathbf{S}} = -\gamma \mathbf{S} \times (\mathbf{H}_{eff} + \mathbf{L}) + \alpha \mathbf{S} \times \dot{\mathbf{S}} \tag{4.2}$$

where $\mathbf{L}$ is a random field characterizing the thermal fluctuation of finite temperature. Although the thermal average of $L(\mathbf{r}, t)$ is zero, the correlation is nonvanishing, satisfying the fluctuation-dissipation relation

$$\left\langle L^i(r,t) L^j(r',t') \right\rangle = \frac{\alpha k_B T}{\gamma} \delta_{ij} \delta_{rr'} \delta_{tt'} \tag{4.3}$$

This nonzero correlation guarantees the corresponding thermal equilibrium satisfies the Boltzmann distribution. We can numerically integrate this equation of motion by the means of stochastic integral, and study the effects of finite temperature

In our simulations, we generalized all parameters in the unit of energy. Then we set $J = 1$, $D = 0.3$, the external field $H = 0.08$.

Furthermore, we also develop two different methods to plot the Skyrmion dynamics. One is the color plot, it plots only z component of the magnetization. The other one is the vector plot, it plots the in plane component by arrows and different color to illustrate the direction and value of the magnetization. As shown in Fig. 4.1, we just choose some random places to plot the Skyrmion, on the color plot we have Skyrmion that all spins point up at the edge of it and spin points down at the center. And on the

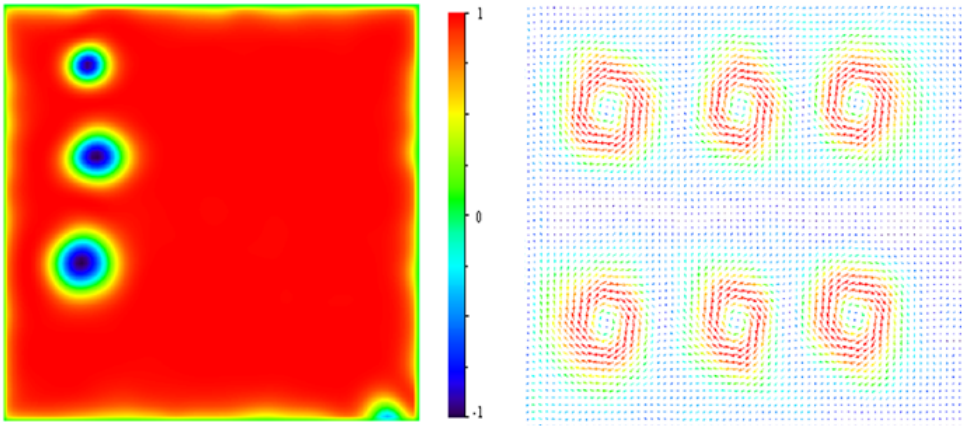

Figure 4.1: Color plot and vector plot of Skyrmion.

vector plot we can see the in plane spin from the center to the edge of Skyrmion.

4.2 Skyrmion Dynamics Simulation

4.2.1 Skyrmion Dynamics with Spinwave

We use open boundary condition in this case to simulate the spin waves or magnons behavior in the presence of Skyrmion. The rectangle shape on the left represents the contact that without a DM interaction. At first we have a Skyrmion in the middle, and then we make a small perturbation at the left edge of the contact, the amplitude A is $< s_x + s_y >= 0.06$. This small perturbation will generate a spin wave propagate to the right. We set the damping constant to 0.0001 to avoid an attenuation of the spin wave. After the spin wave hit the Skyrmion position, there's an obviously scattering happened as shown in Fig. 4.2. In the case without a Skyrmion, the spin wave just propagate straight to the right.

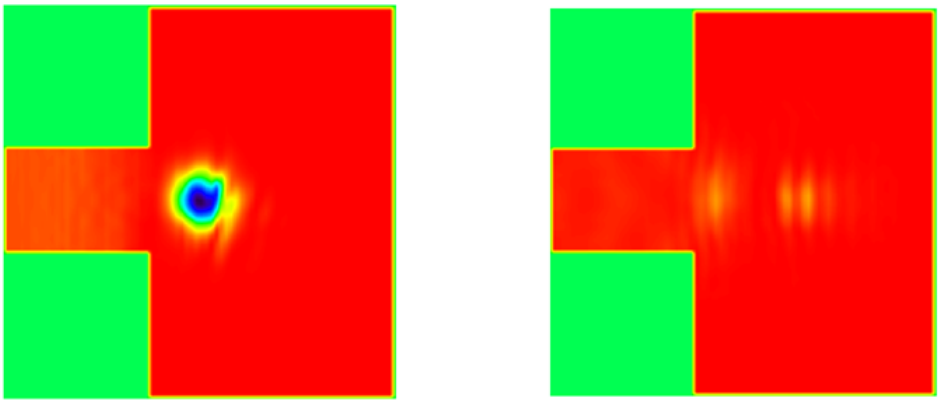

Figure 4.2: Spin wave scattering by Skyrmion, the left plot is the case with a Skyrmion, the right plot is the case without a Skyrmion.

However, the scattering angle is not a constant. After test different pairs of parameters, the angle seems strongly dependent on the size R of Skyrmion, where R is depend on $\frac{J}{D}$. A plot of different scattering angles with different size of Skyrmion are shown in Fig. 4.3

4.2.2 Topological Hall Effect Simulation

A Skyrmion Topological Hall effect numerical simulation is shown in Fig4.4. The Topological Hall Effect is induced by the conduction electrons go through a Skyrmion, the electron will pick up a Berry phase and influenced by the effective field that generated by the Skyrmion. When an electron system is coupled to the spin system, the electron spin and the on-site local spin are coupled via Hund's rule coupling:

$$H_{\mathrm{eS}} = -J_{\mathrm{H}} \sum_{i} c_i^{\dagger} \sigma c_i \cdot \mathbf{S}_i. \tag{4.4}$$

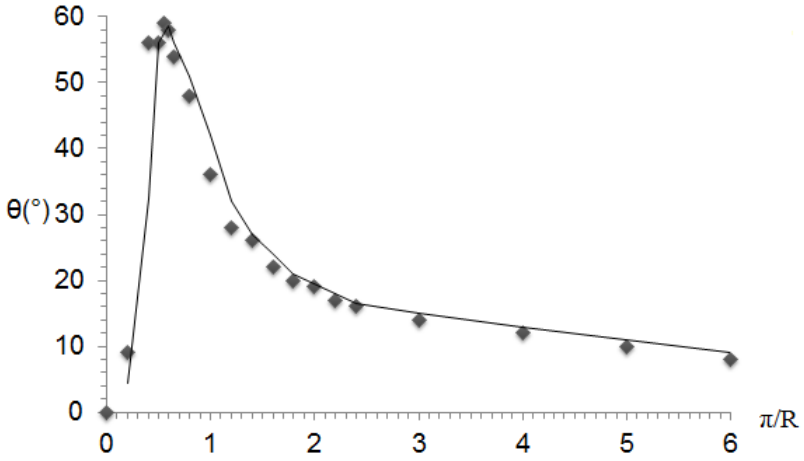

Figure 4.3: The curve of the relationship between the scattering angle and the k($= \frac{\pi}{R}$) vector.

To couple the spin texture $\{\mathbf{S}_i\}$ with a tight-binding model, the Hamiltonian of the electron system is

$$H = \epsilon_i \sum_i c_i^\dagger c_i - t \sum_{\langle i,j \rangle} \left(c_i^\dagger c_j + \text{h.c.} \right) + - J_\text{H} \sum_i c_i^\dagger \sigma c_i \cdot \mathbf{S}_i \tag{4.5}$$

Since these are metallic systems, we formulate and obtain a linear response solution to the standard non-equilibrium Green function (NEGF) equations. For horizontal current injection and extraction, open system boundary conditions are applied at the right and left of the tight-binding mesh. Vertical injection can be modeled with boundary conditions previously applied to injection into the surface of a topological insulator. For the contacts at the left and right, the retarded Green function is $\mathbf{G}^R = [\epsilon - \mathbf{H} - \mathbf{\Sigma}_L - \mathbf{\Sigma}_R]^{-1}$ where $\Sigma_{L,R}$ stands for the self-energy terms given by the left and right semi-infinite open boundaries. Using the recursive Green function algorithm, one can obtain the diagonal blocks, $\mathbf{G}^R_{n,n}$, and the first column, $\mathbf{G}^R_{n,1}$, respectively. Thus, the left-injected spectral

function can be given as

$$\mathbf{A}^{L}_{n,n} = \mathbf{G}^{R}_{n,1}\mathbf{\Gamma}_{1,1}\mathbf{G}^{R\dagger}_{1,n} \tag{4.6}$$

in which each on-site block is a 2×2 matrix in the spin basis. The total spectral function is given as

$$\mathbf{A}_{n,n} = \mathbf{A}^{L}_{n,n} + \mathbf{A}^{R}_{n,n} = i\left(\mathbf{G}^{R}_{n,n} - \mathbf{G}^{A}_{n,n}\right) \tag{4.7}$$

where $\mathbf{G}^{A} = \mathbf{G}^{R\dagger}$ is the advanced Green's function. In the linear-response limit, small bias is applied, so the the Fermi distribution of the left electrode, f_L, and the right electrode, f_R can be expanded to first order in the bias μ,

$$f_L = f_0 + \left(\frac{-\partial f_0}{\partial\epsilon}\right)\frac{\Delta\mu}{2} \tag{4.8}$$

$$f_R = f_0 - \left(\frac{-\partial f_0}{\partial\epsilon}\right)\frac{\Delta\mu}{2}. \tag{4.9}$$

Thus, the lesser Green's function can be simplified to

$$\mathbf{G}^{<}_{n,n} = if_L\mathbf{A}^{L}_{n,n} + if_R\mathbf{A}^{R}_{n,n} = if_0\mathbf{A}_{n,n} - \frac{\Delta\mu}{2}\left(\frac{\partial f_0}{\partial\epsilon}\right)\left(2\mathbf{A}^{L}_{n,n} - \mathbf{A}_{n,n}\right). \tag{4.10}$$

The local charge density can be written as

$$n_{n,n} = n^{0}_{n,n} + \Delta n_{n,n} = -i\int\frac{d\epsilon}{2\pi}\mathrm{Tr}\left\{\mathbf{G}^{<}_{n,n}(\epsilon)\right\} \tag{4.11}$$

where

$$\Delta n_{n,n} = \int\frac{d\epsilon}{2\pi}\left(2\mathbf{A}^{L}_{n,n} - \mathbf{A}_{n,n}\right)\left(\frac{-\partial f_0}{\partial\epsilon}\right)\frac{\Delta\mu}{2}. \tag{4.12}$$

At equilibrium, the linear response of the charge to a small shift in the local chemical potential, $\delta\mu_{n,n}$, is

$$\Delta n_{n,n} = \int\frac{d\epsilon}{2\pi}\mathbf{A}_{n,n}\left(\frac{-\partial f_0}{\partial\epsilon}\right)\delta\mu_{n,n}. \tag{4.13}$$

Comparing Eq. 4.12 and Eq. 4.13, the local non-equilibrium chemical potential is

$$\delta\mu_{n,n} = \frac{\Delta n_{n,n}}{\int\frac{d\epsilon}{2\pi}A_{n,n}\left(\frac{-\partial f_0}{\partial\epsilon}\right)}. \tag{4.14}$$

Letting $t = 1.5\,\text{eV}$, $J_\text{H} = 1.0\,\text{eV}$, $T = 300\,\text{K}$, $\Delta\mu = 0.1\,\text{V}$, a numerical simulation of the topological Hall voltage is shown in Fig. 4.4. This is the first such explicit, numerical simulation of the topological Hall effect resulting from a Skyrmion. The transverse

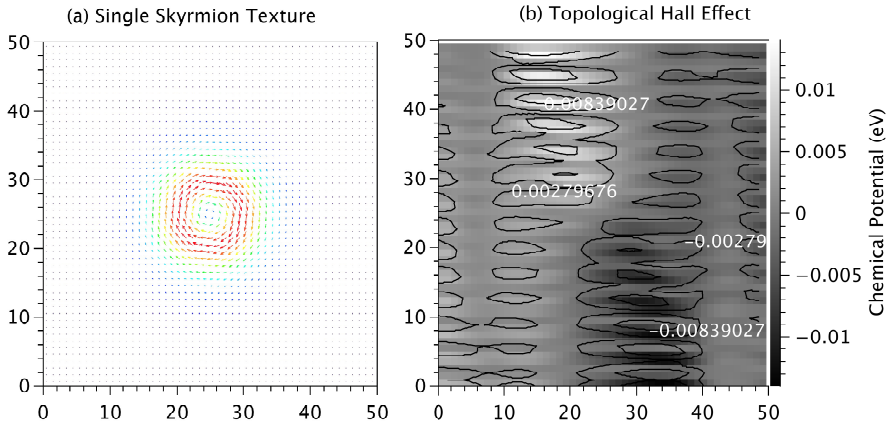

Figure 4.4: Topological Hall effect close to a single skyrmion. In this simulation, the nearest neighbor coupling term is $t = 1.5J_H$, $J_H = 1.0\,\text{eV}$, and $T = 300\,\text{K}$. A voltage drop of $0.1\,\text{V}$ is applied from the left to the right. Close to the skyrmion texture, the transverse chemical potential demonstrates a Hall voltage signal of $0.03\,\text{V}$.

difference in the chemical potential is clear in Fig. 4.4(b). This difference in chemical potential is the Hall voltage that is measured in a 4-point probe measurement. By the Topological Hall Effect, the reading of a Skyrmion is possible.

4.3 Skyrmion-based Device Architecture

Since the simulation shows some interesting properties of Skyrmion, it's possible for us to propose some Skyrmion-based devices. A very unique propertiy of Skyrmion is the threshold current needed to move a Skyrmion is about 5 orders small compare to the domain wall motion. Inspired by the domain wall racetrack memory[5], a Skyrmion-based racetrack memory is proposed. The advantage of a racetrack memory is we can make 3D architecture as shown in Fig. 4.5 E, so the density can be increased. And since Skyrmion has relatively small size usually range from 10nm to 100nm, we can make devices with higher density. Also, due to the small critical current, this kind of device will be more energy efficient. A schematic structure of Skyrmion-based racetrack memory is shown in Fig. 4.6. We replace the domain wall with Skyrmion arrays. A write head and read head is on the bottom. The writing process may use the current pulse to generating a single Skyrmion, and the reading process may achieve by the topological hall effect. A current comes from the left or right will move the whole Skyrmion array so that we can read different part of the array.

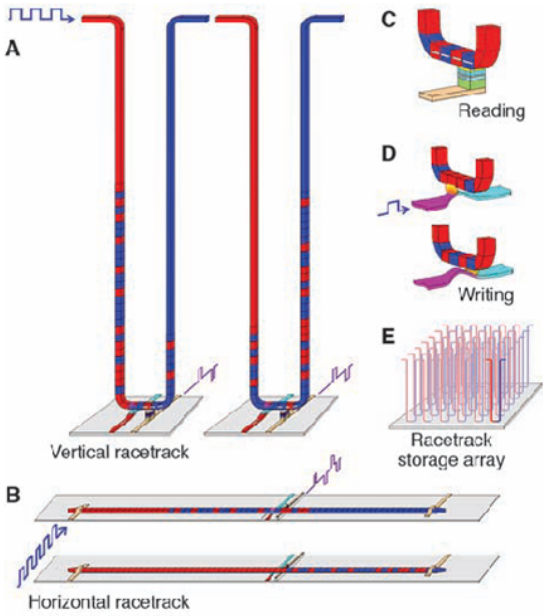

Figure 4.5: Domain wall racetrack memory.[5]

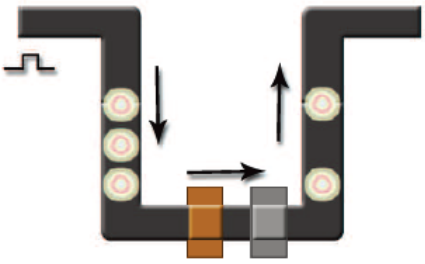

Figure 4.6: Skyrmion-based racetrack memory.

Chapter 5

Conclusion

5.1 Summary

We developed a simulation tool that have the capability to simulate Skyrmion dymacis at finite temperature. Skyrmion dynamics are simulated by micromagnetic simulations. The Skyrmion-magnon scattering are shown by micromagnetic simulations. The scattering angle is strongly depend on the size of Skyrmion. A topological hall effect is shown to be a method to read a Skyrmion. Based on these simulations, a Skyrmion-based device is proposed.

5.2 Future Plans

Micromagnetic simulations is expected to do for the specific structure we proposed. We will continue finding new methods to reduce the energy needed to create a single Skyrmion based on our code. Also, the inner physics of magnon-Skyrmion scattering and Skyrmion creation process will be studied in the future since it's important to understand these physics before build real devices. Some other architectures may be

proposed and simulated based on the spin wave dynamics, it's possible to build logic circuit based on the spin wave structure. New code that combines the first principle may be developed to calculate the exchange constant and DM constant of different materials. We also plan to extend our code capability to simulate some 3D models, by using a 3D model we could simulate more complicated Skyrmion Lattice and Skyrmion-based devices.

Bibliography

[1] S. Seki, X. Z. Yu, S. Ishiwata, and Y. Tokura. Observation of skyrmions in a multiferroic material. *Science*, 336(6078):198 – 201, 2012.

[2] F. Jonietz, S. Mühlbauer, C. Pfleiderer, A. Neubauer, W. Münzer, A. Bauer, T. Adams, R. Georgii, P. Böni, R. A. Duine, K. Everschor, M. Garst, and A. Rosch. Spin transfer torques in MnSi at ultralow current densities. *Science*, 330(6011):1648–1651, December 2010. PMID: 21164010.

[3] T. Schulz, R. Ritz, A. Bauer, M. Halder, M. Wagner, C. Franz, C. Pfleiderer, K. Everschor, M. Garst, and A. Rosch. Emergent electrodynamics of skyrmions in a chiral magnet. *Nature Physics*, 8(4):301–304, April 2012.

[4] K Everschor. Current-induced dynamics of chiral magnetic structures: Skyrmions, emergent electrodynamics and spin-trasfer torques. *PhD thesis, University of Koln, Germany*.

[5] S. S. P. Parkin, M. Hayashi, and L. Thomas. Magnetic domain-wall racetrack memory. *Science*, 320(5873):190–194, April 2008.

[6] Shinji Yuasa, Taro Nagahama, Akio Fukushima, Yoshishige Suzuki, and Koji Ando. Giant room-temperature magnetoresistance in single-crystal Fe/MgO/Fe magnetic tunnel junctions. *Nat Mater*, 3:868–871.

[7] Max M. Shulaker, Gage Hills, Nishant Patil, Hai Wei, Hong-Yu Chen, H.-S. Philip Wong, and Subhasish Mitra. Carbon nanotube computer. *Nature*, 501:526–530.

[8] Richard P. Feynman. Simulating physics with computers. *Int J Theor Phys*, 21:467–488.

[9] Junichi Iwasaki, Masahito Mochizuki, and Naoto Nagaosa. Current-induced skyrmion dynamics in constricted geometries. *Nature Nanotechnology*, 8(10):742–747, October 2013.

[10] J. Sampaio, V. Cros, S. Rohart, A. Thiaville, and A. Fert. Nucleation, stability and current-induced motion of isolated magnetic skyrmions in nanostructures. *Nature Nanotechnology*, advance online publication, October 2013.

[11] Tôru Moriya. Anisotropic superexchange interaction and weak ferromagnetism. *Physical Review*, 120(1):91–98, October 1960.

[12] I. Dzyaloshinsky. A thermodynamic theory of weak ferromagnetism of antiferromagnetics. *Journal of Physics and Chemistry of Solids*, 4:241–255.

[13] T. H. R. Skyrme. A non-linear field theory. *Proceedings of the Royal Society of London. Series A. Mathematical and Physical Sciences*, 260(1300):127–138, February 1961.

[14] Niklas Romming, Christian Hanneken, Matthias Menzel, Jessica E. Bickel, Boris Wolter, Kirsten von Bergmann, André Kubetzka, and Roland Wiesendanger. Writing and deleting single magnetic skyrmions. *Science*, 341(6146):636–639, August 2013. PMID: 23929977.

[15] S. Mühlbauer, B. Binz, F. Jonietz, C. Pfleiderer, A. Rosch, A. Neubauer, R. Georgii, and P. Böni. Skyrmion lattice in a chiral magnet. *Science*, 323(5916):915–919, February 2009. PMID: 19213914.

[16] X. Z. Yu, Y. Onose, N. Kanazawa, J. H. Park, J. H. Han, Y. Matsui, N. Nagaosa, and Y. Tokura. Real-space observation of a two-dimensional skyrmion crystal. *Nature*, 465(7300):901–904, June 2010.

[17] Jung Hoon Han, Jiadong Zang, Zhihua Yang, Jin-Hong Park, and Naoto Nagaosa. Skyrmion lattice in a two-dimensional chiral magnet. *Physical Review B*, 82(9):094429, September 2010.

[18] N. Kanazawa, Y. Onose, T. Arima, D. Okuyama, K. Ohoyama, S. Wakimoto, K. Kakurai, S. Ishiwata, and Y. Tokura. Large topological hall effect in a short-period helimagnet MnGe. *Phys. Rev. Lett.*, 106(15):156603, April 2011.

[19] Jiadong Zang, Maxim Mostovoy, Jung Hoon Han, and Naoto Nagaosa. Dynamics of skyrmion crystals in metallic thin films. *Physical Review Letters*, 107(13):136804, September 2011.

[20] J. S. White, I. Levatić, A. A. Omrani, N. Egetenmeyer, K. Prša, I. Živković, J. L. Gavilano, J. Kohlbrecher, M. Bartkowiak, H. Berger, and H. M. Rønnow. Electric field control of the skyrmion lattice in Cu2OSeO3. *Journal of Physics: Condensed Matter*, 24(43):432201, October 2012.

[21] X. Z. Yu, N. K. anazawa, Y. Onose, K. Kimoto, W. Z. Zhang, S. Ishiwata, Y. Matsui, and Y. Tokura. Near room-temperature formation of a skyrmion crystal in thin-films of the helimagnet FeGe. *Nat Mater*, 10(2):106 – 109, 2011.

[22] S. X. Huang and C. L. Chien. Extended skyrmion phase in epitaxial FeGe(111) thin films. *Phys. Rev. Lett.*, 108(26):267201, June 2012.

[23] Stefan Heinze, Kirsten von Bergmann, Matthias Menzel, Jens Brede, André Kubetzka, Roland Wiesendanger, Gustav Bihlmayer, and Stefan Blügel. Spontaneous atomic-scale magnetic skyrmion lattice in two dimensions. *Nature Physics*, 7(9):713–718, September 2011.

[24] Wei Han, K. Pi, K. M. McCreary, Yan Li, Jared J. I. Wong, A. G. Swartz, and R. K. Kawakami. Tunneling spin injection into single layer graphene. *Physical Review Letters*, 105(16):167202, October 2010.

[25] Wei Han and R. K. Kawakami. Spin relaxation in single-layer and bilayer graphene. *Physical Review Letters*, 107(4):047207, July 2011.

[26] T.H.R. Skyrme. A unified field theory of mesons and baryons. *Nuclear Physics*, 31:556–569, March 1962.

[27] Naoto Nagaosa, Jairo Sinova, Shigeki Onoda, A. H. MacDonald, and N. P. Ong. Anomalous hall effect. *Reviews of Modern Physics*, 82(2):1539–1592, May 2010.

[28] T. Jungwirth, Qian Niu, and A. H. MacDonald. Anomalous hall effect in ferromagnetic semiconductors. *Physical Review Letters*, 88(20):207208, May 2002.

[29] J.C. Slonczewski. Current-driven excitation of magnetic multilayers. *Journal of Magnetism and Magnetic Materials*, 159(1–2):L1–L7, June 1996.

[30] B. Berg and M. Lüscher. Definition and statistical distributions of a topological number in the lattice o(3) σ-model. *Nuclear Physics B*, 190(2):412–424, August 1981.

[31] Shi-Zeng Lin, Charles Reichhardt, Cristian D. Batista, and Avadh Saxena. Driven skyrmions and dynamical transitions in chiral magnets. *Physical Review Letters*, 110(20), May 2013.

[32] Lingyao Kong and Jiadong Zang. Dynamics of an insulating skyrmion under a temperature gradient. *Physical Review Letters*, 111(6):067203, August 2013.

[33] Keisuke Yamada, Shinya Kasai, Yoshinobu Nakatani, Kensuke Kobayashi, Hiroshi Kohno, André Thiaville, and Teruo Ono. Electrical switching of the vortex core in a magnetic disk. *Nature Materials*, 6(4):270–273, April 2007.

[34] L. Berger. Emission of spin waves by a magnetic multilayer traversed by a current. *Physical Review B*, 54(13):9353–9358, October 1996.

[35] S. Seki, J.-H. Kim, D. S. Inosov, R. Georgii, B. Keimer, S. Ishiwata, and Y. Tokura. Formation and rotation of skyrmion crystal in the chiral-lattice insulator Cu$_2$OSeO$_3$. *Phys. Rev. B*, 85(22):220406, June 2012.

[36] Y. Ishikawa, K. Tajima, D. Bloch, and M. Roth. Helical spin structure in manganese silicide MnSi. *Solid State Communications*, 19(6):525 – 528, 1976.

[37] H. Takizawa, T. Sato, T. Endo, and M. Shimada. High-pressure synthesis and electrical and magnetic properties of MnGe and CoGe with the cubic b20 structure. *Journal of Solid State Chemistry*, 73(1):40 – 46, 1988.

[38] T. Jeong and W. E. Pickett. Implications of the b20 crystal structure for the magnetoelectronic structure of MnSi. *Phys. Rev. B*, 70(7):075114, August 2004.

[39] José Luis García-Palacios and Francisco J. Lázaro. Langevin-dynamics study of the dynamical properties of small magnetic particles. *Physical Review B*, 58(22):14937–14958, December 1998.

[40] M. Finazzi, M. Savoini, A. R. Khorsand, A. Tsukamoto, A. Itoh, L. Duò, A. Kirilyuk, Th. Rasing, and M. Ezawa. Laser-induced magnetic nanostructures with tunable topological properties. *Physical Review Letters*, 110(17):177205, April 2013.

[41] J. Beille, J. Voiron, and M. Roth. Long period helimagnetism in the cubic b20 FexCo1-xSi and CoxMn1-x si alloys. *Solid State Communications*, 47(5):399 – 402, 1983.

[42] T. Adams, A. Chacon, M. Wagner, A. Bauer, G. Brandl, B. Pedersen, H. Berger, P. Lemmens, and C. Pfleiderer. Long-wavelength helimagnetic order and skyrmion lattice phase in Cu2OSeO3. *Phys. Rev. Lett.*, 108(23):237204, June 2012.

[43] Daizaburo Shinoda and Sizuo Asanabe. Magnetic properties of silicides of iron group transition elements. *J. Phys. Soc. Jpn.*, 21:555, January 1966.

[44] J. W. Kłos, D. Kumar, M. Krawczyk, and A. Barman. Magnonic band engineering by intrinsic and extrinsic mirror symmetry breaking in antidot spin-wave waveguides. *Scientific Reports*, 3, August 2013.

[45] Alexander Khitun. Magnonic holographic devices for special type data processing. *Journal of Applied Physics*, 113(16):164503, 2013.

[46] Shi-Zeng Lin, Charles Reichhardt, and Avadh Saxena. Manipulation of skyrmions in nanodisks with a current pulse and skyrmion rectifier. *Applied Physics Letters*, 102(22):222405, 2013.

[47] Ya. B. Bazaliy, B. A. Jones, and Shou-Cheng Zhang. Modification of the landau-lifshitz equation in the presence of a spin-polarized current in colossal- and giant-magnetoresistive materials. *Physical Review B*, 57(6):R3213–R3216, February 1998.

[48] Y. Onose, Y. Okamura, S. Seki, S. Ishiwata, and Y. Tokura. Observation of magnetic excitations of skyrmion crystal in a helimagnetic insulator Cu2OSeO3. *Phys. Rev. Lett.*, 109(3):037603, July 2012.

[49] Shi-Zeng Lin, Charles Reichhardt, Cristian D. Batista, and Avadh Saxena. Particle model for skyrmions in metallic chiral magnets: Dynamics, pinning, and creep. *Physical Review B*, 87(21), June 2013.

[50] N. Kanazawa, J.-H. Kim, D. S. Inosov, J. S. White, N. Egetenmeyer, J. L. Gavilano, S. Ishiwata, Y. Onose, T. Arima, B. Keimer, and Y. Tokura. Possible skyrmion-lattice ground state in the b20 chiral-lattice magnet MnGe as seen via small-angle neutron scattering. *Physical Review B*, 86(13):134425, October 2012.

[51] X. Z. Yu, N. Kanazawa, W. Z. Zhang, T. Nagai, T. Hara, K. Kimoto, Y. Matsui, Y. Onose, and Y. Tokura. Skyrmion flow near room temperature in an ultralow current density. *Nature Communications*, 3:988, August 2012.

[52] Youngbin Tchoe and Jung Hoon Han. Skyrmion generation by current. *Physical Review B*, 85(17):174416, May 2012.

[53] W. Munzer, A. Neubauer, T. Adams, S. Muhlbauer, C. Franz, F. Jonietz, R. Georgii, P. Boni, B. Pedersen, M. Schmidt, A. Rosch, and C. Pfleiderer. Skyrmion lattice in the doped semiconductor Fe1xCoxSi. *Phys. Rev. B*, 81(4):041203, January 2010.

[54] C. Pfleiderer, T. Adams, A. Bauer, W. Biberacher, B. Binz, F. Birkelbach, P. Böni, C. Franz, R. Georgii, M. Janoschek, F. Jonietz, T. Keller, R. Ritz, S. Mühlbauer,

W. Münzer, A. Neubauer, B. Pedersen, and A. Rosch. Skyrmion lattices in metallic and semiconducting b20 transition metal compounds. *Journal of Physics: Condensed Matter*, 22(16):164207, 2010.

[55] Su Do Yi, Shigeki Onoda, Naoto Nagaosa, and Jung Hoon Han. Skyrmions and anomalous hall effect in a dzyaloshinskii-moriya spiral magnet. *Physical Review B*, 80(5):054416, August 2009.

[56] Albert Fert, Vincent Cros, and J. Sampaio. Skyrmions on the track. *Nature nanotechnology*, 8(3):152–156, 2013.

[57] R Rajaraman. *Solitons and Instantons*. North-Holland, Amsterdam, 1987.

[58] J. Teyssier, E. Giannini, V. Guritanu, R. Viennois, D. van der Marel, A. Amato, and S. N. Gvasaliya. Spin-glass ground state in Mn1xCoxSi. *Phys. Rev. B*, 82(6):064417, August 2010.

[59] U. K. Rößler, A. N. Bogdanov, and C. Pfleiderer. Spontaneous skyrmion ground states in magnetic metals. *Nature*, 442(7104):797–801, August 2006.

[60] Claude Chappert, Albert Fert, and Frédéric Nguyen Van Dau. The emergence of spin electronics in data storage. *Nature materials*, 6(11):813–823, 2007.

[61] Junichi Iwasaki, Aron J. Beekman, and Naoto Nagaosa. Theory of magnon-skyrmion scattering in chiral magnets. arXiv e-print 1309.2361, September 2013.

[62] A. Neubauer, C. Pfleiderer, B. Binz, A. Rosch, R. Ritz, P. G. Niklowitz, and P. Böni. Topological hall effect in the a phase of MnSi. *Physical Review Letters*, 102(18):186602, May 2009.

[63] Junichi Iwasaki, Masahito Mochizuki, and Naoto Nagaosa. Universal current-velocity relation of skyrmion motion in chiral magnets. *Nature Communications*, 4:1463, February 2013.

[64] Tru Moriya. Anisotropic superexchange interaction and weak ferromagnetism. 120:9198.

[65] Tadashi Arai. Exchange interaction and heisenberg's spin hamiltonian. *Phys. Rev.*, 126:471–488.

[66] W. Heisenberg. Mehrkrperproblem und resonanz in der quantenmechanik. *Z. Physik*, 38:411–426.

[67] X. Z. Yu, N. Kanazawa, Y. Onose, K. Kimoto, W. Z. Zhang, S. Ishiwata, Y. Matsui, and Y. Tokura. Near room-temperature formation of a skyrmion crystal in thin-films of the helimagnet FeGe. *Nat Mater*, 10:106–109.

[68] P. a. M. Dirac. On the theory of quantum mechanics. *Proc. R. Soc. Lond. A*, 112:661–677.